OPEN ACCESS

Degradation Effects at the Porous Transport Layer/Catalyst Layer Interface in Polymer Electrolyte Membrane Water Electrolyzer

Journal of The Electrochemical Society, 2023 **170** 034508

Degradation Effects at the Porous Transport Layer/Catalyst Layer Interface in Polymer Electrolyte Membrane Water Electrolyzer

Chang Liu,[1,2,a,z] Meital Shviro,[1,a] Guido Bender,[3] Aldo S. Gago,[4] Tobias Morawietz,[4,5] Michael J. Dzara,[6] Indro Biswas,[4] Pawel Gazdzicki,[4] Zhenye Kang,[3] Sarah F. Zaccarine,[6] Svitlana Pylypenko,[6] K. Andreas Friedrich,[4,7] Marcelo Carmo,[1,8,b] and Werner Lehnert[1,2]

[1]*Forschungszentrum Jülich GmbH, Institute of Energy and Climate Research (IEK-14): Electrochemical Process Engineering, 52425, Jülich, Germany*
[2]*Modeling in Electrochemical Process Engineering, RWTH Aachen University, 52056, Aachen, Germany*
[3]*Chemistry and Nanoscience Center, National Renewable Energy Laboratory (NREL), Golden, CO 80401, United States of America*
[4]*Institute of Engineering Thermodynamics, German Aerospace Center (DLR), Pfaffenwaldring 38-40, 70569, Stuttgart, Germany*
[5]*Faculty of Science, Energy and Building Services, Esslingen University of Applied Sciences, Kanalstraße 33, 73728, Esslingen am Neckar, Germany*
[6]*Department of Chemistry, Colorado School of Mines, Golden, CO 80401, United States of America*
[7]*Institute for Building Energetics, Thermotechnology and Energy Storage (IGTE), University of Stuttgart, Pfaffenwaldring 31, 70569, Stuttgart, Germany*
[8]*Mechanical and Materials Engineering, Queen's University, Kingston, ON K7L 3N6, Canada*

The porous transport layer (PTL)/catalyst layer (CL) interface plays a crucial role in the achievement of high performance and efficiency in polymer electrolyte membrane water electrolyzers (PEMWEs). This study investigated the effects of the PTL/CL interface on the degradation of membrane electrode assemblies (MEAs) during a 4000 h test, comparing the MEAs assembled with uncoated and Ir-coated Ti PTLs. Our results show that compared to an uncoated PTL/CL interface, an optimized interface formed when using a platinum group metal (PGM) coating, i.e., an iridium layer at the PTL/CL interface, and reduced the degradation of the MEA. The agglomeration and formation of voids and cracks could be found for both MEAs after the long-term test, but the incorporation of an Ir coating on the PTL did not affect the morphology change or oxidation of IrO_x in the catalyst layer. In addition, our studies suggest that the ionomer loss and restructuring of the anodic MEA can also be reduced by Ir coating of the PTL/CL interface. Optimization of the PTL/CL interface improves the performance and durability of a PEMWE.
 [DOI: 10.1149/1945-7111/acc1a5]

Manuscript submitted January 17, 2023; revised manuscript received February 19, 2023. Published March 29, 2023.

Supplementary material for this article is available online

Hydrogen production via water electrolysis is a promising energy storage technology that can be coupled with renewable energy sources such as wind or solar.[1–3] Compared to traditional alkaline water electrolysis, polymer electrolyte membrane (PEM) electrolysis offers several advantages, including high hydrogen purity, fast dynamic response, and a compact design.[4,5] To date, its advancement has been limited by stability issues, and the degradation mechanisms of cell and stack components at low loading and under dynamic operation in particular are not fully understood. Much work until now has focused on investigating the degradation of different components of electrolysis cells.[6–13] The main degradation phenomena for PEM water electrolyzer components include structural changes to the catalysts, deactivation of the electrolyte, loss of performance due to ion impurities in the feed water, and the corrosion and passivation of titanium-based bipolar plates (BPPs) and porous transport layers (PTLs).

Iridium-based electrocatalysts are most widely used for the oxygen evolution reaction (OER) at the anode of PEM electrolyzers due to their superior activity and durability.[14] Nonetheless, future generation membrane electrode assemblies (MEAs) are expected to require significant loading reductions for PEM water electrolyzers in order to become economically-viable, which increases the requirements for electrode durability due to less catalyst material being available to serve as a material buffer. The research community has started to address this need through ex situ and in situ studies. For instance, several rotating disk electrode (RDE) durability studies have investigated the relative stabilities of catalysts and evaluated the mechanisms of catalyst degradation.[15–17] Alia et al.[16] carried out a series of experiments to analyze the durability of iridium-based catalysts in both RDE and single cells. They found that the loss of mass activity began at a moderate potential (1.4 to 1.6 V), and the degradation to be driven by iridium dissolution at high potential (>1.8 V) when using an RDE. Various single cell studies investigated the performance and durability of MEAs and described iridium dissolution, changes in the catalyst layer (CL) structure, and the effects of loading and operating conditions on degradation.[6–8,18] It was found in Alia's[14] study that low catalyst loading, high cell potential and dynamic operation resulted in increased durability losses. Thicker catalyst layers provide an iridium buffer that can slow and mask the decrease in cell performance. In addition, their study showed that iridium and interfacial deterioration of the catalyst/ionomer/membrane interface may also contribute to durability losses.

Catalyst agglomeration and morphology changes can also lead to MEA degradation. The increase in single catalyst particle sizes due to sintering or crystal size growth over time leads to a significant loss in electrochemically-active surface areas.[9] This process occurs on the cathode as well as on the anode. For example, Pt agglomeration combined with a cathodic platinum crystal size increase was reported after long-term testing by several groups.[6,8] In a previous study, we reported that the platinum crystal sizes at the cathode increased from 3.5 nm to 7.8 nm after operation at 2 $A \cdot cm^{-2}$ over 1150 h.[6] At the anode, the applied voltage accelerates the degradation of the ionomer, which eventually causes a disintegration of the catalyst layer.[19] The stability of IrO_2 may also be reflected in changes to the catalyst material's morphology. Using RDE tests,

[a]Present address: Chemistry and Nanoscience Center, National Renewable Energy Laboratory (NREL), Golden, CO 80401, USA.
[b]Present address: NEL Hydrogen, Wallingford, Connecticut, 06492, USA.
[z]E-mail: chang.liu@nrel.gov; changliu01102@gmail.com

Povia et al.[20] showed that IrO_2 produced by heat-treating preserves its original morphology over a square potential wave between 1.0 and 1.6 V vs RHE for 500 cycles, holding at each U-value for 10 s stability tests. Another study by Jovanovic et al.[21] showed that the OER activity of IrO_2 is lower after exposure to 10000 cycles between 1 and 1.6 V vs SCE with a scan rate 1 V s^{-1}, with no morphological difference being visible. Implementing a single cell study, Rakousky et al.[6] demonstrated that the crystal size of the anodic catalyst (IrO_2) remained constant during a 1000 h test at a constant current density of 2 A·cm^{-2}. No change in the morphology of the anode catalyst layer was observed. In contrast, however, a study by Siracusano et al.,[8] during which a cell was exposed to 1000 h at 1 A·cm^{-2}, indicated that the $IrRuO_x$ anode catalyst layer was less agglomerated at the end of the study period. Another mechanism that can contribute to reduced kinetics is the leaching of ionomers out of the catalyst layer which results in lower site access and a decline in performance.[22] The Nafion ionomer is an ionic conductor that extends proton conduction from the bulk of the PEM membrane to the surface of the catalyst. The ionomer also serves as a binder and helps create a three-dimensional catalyst layer structure that permits electron, water, and gas transport and provides a certain degree of mechanical stability. The loss and degradation of ionomer in the catalyst layer limits the access of protons to otherwise active reaction sites. This process leads to a lower catalyst utilization, a loss of performance, or even a total failure of the cell.[23]

Although many efforts have been devoted to investigating the degradation of each component, significantly fewer studies have looked into how the interface between two components, such as the PTL/CL interface, could affect the long-term durability and catalyst layer morphology.[24–26] For instance, Schuler et al.[24] reported that the interfacial contact area between the catalyst layer and PTL determines the contact resistance and plays an essential role in limiting the catalyst utilization. In turn, Lopata et al.[25] showed that strong correlations exist between PTL surface properties and cell performance, specifically when the anode catalyst loading (< 0.1 mg_{Ir}·cm^{-2}) is very low. However, when the anode catalyst loading is high (>0.5 mg_{Ir}·cm^{-2}), the cell performance variation between the same PTLs is very small. In general, the interface between the PTL and CL influences the overpotentials in the cell, including activation and ohmic overpotential. Each of the overpotentials of the cell can be reduced using specific strategies such as coating,[6,27–29] etching,[30] or advancing material properties, i.e., adding MPLs to PTLs.[31–33] A recent study reported that the specific surface area of titanium-based PTL fibers can be increased by using femtosecond laser-induced surface structuring. The electrochemical characterization and short-term stress measurements show that the laser-structuring of the PTL surface improved the cell performance, i.e., the cell voltage was reduced by approximately 30 mV after 100 h at 4 A·cm^{-2}.[26] In summary, several current research efforts have investigated the effects of material and interface properties as well as component interactions on performance, but none of these considered the performance effects that originate from material or component property changes due to long-term operation. Recent PTL studies show that both iridium and platinum coating can be used as protective layers to safeguard the PTLs from passivation and improve cell performance and durability.[28,29,34–36] Our recent study showed that the Ir protective layer on the PTL not only decreases the ohmic resistance significantly, but moreover, the OER activity of the iridium layer makes it promising as a cost-effective catalyst layer.[29] The proper construction of the interface between the PTL and CL plays a crucial role in achieving superior durability and efficiency in a PEM water electrolyzer.

In this work, we investigated the effects of a PTL/CL interface on MEA morphology and degradation after a long-term test for a PEM water electrolyzer. The performance effects on the cells constructed with or without an Ir coating between the PTL/CL interface, the morphology and oxidation change of IrO_x, and ionomer loss of the anode catalyst layer after long-term operation are discussed. Our study demonstrates that the proper design of the PTL/CL interface, e.g., using Ir coating on the PTL, reduced the degradation of the anodic catalyst layer. This study highlights not only the properly designing the interface between the catalyst and transport layer to ensure higher performance, but more importantly, to reduce the degradation of the catalyst layer in PEM water electrolyzers. The results of this work will contribute to a better understanding of the PTL/CL interface design and elucidate the MEA degradation mechanism for PEM water electrolyzers during long-term operation.

Experimental

Materials.—The MEA samples were manufactured using a doctor blade and decal coating method followed by a hot press transfer. The target catalyst loadings for the MEAs were ∼0.8 mg·cm^{-2} Pt/C (HiSPEC 9100, Johnson & Matthey) for the cathode and ∼2.2 mg·cm^{-2} IrO_2 (Alfa Aesar, Premion, 99.99%) for the anode. Ti felt PTLs with a thickness of 250 μm and 56% nominal porosity (2GDL10–0.25, Bekaert, Belgium) were used as anode PTLs. Carbon papers (TGP-H 120, Toray®) with a thickness of 350 μm were used as the cathode GDLs. The material of the cell that was assembled with the clean uncoated titanium PTL at the anode was compared in this work to those of the cell that were assembled with the iridium coated PTL at the anode. The cleaning procedure for the PTL prior to coating and sputtering procedures were reported in a previous publication.[28,29] The Ir was coated on both sides of PTL with 0.1 mg·cm^{-2} Ir totally. Comparing to the Ir layer on Ti felt reported from another study,[37] the entire surfaces of Ir coated PTL in our study are homogeneously covered with Ir. The details of materials are displayed in Table I.

Electrochemical measurements.—The active area of the cells was 17.64 cm^2 and bipolar plates were coated with Pt and Au on for the anode and cathode, respectively. The long-term measurements were conducted at 80 °C under ambient pressure and a constant voltage of 2 V for 4000 h, circulating 18.2 MΩ·cm of deionized water at 25 ml·min^{-1} individually through the cathode and anode compartments. Polarization curves were recorded prior to and after the long-term measurement. The polarization curve measurements started from open circuit, first increasing the current density in 0.025 A·cm^{-2} steps to 0.1 A·cm^{-2}, and then in 0.2 A·cm^{-2} steps until reaching the limiting cell voltage of 2 V. Each step was held for 5 min.

Characterization of MEA components.—Several techniques were used to compare the morphological and physiochemical properties of pristine and aged MEAs. The aged MEA materials were extracted by disassembling the cells, i.e., separating the PTLs from the MEAs after 4000 h of durability testing.

Scanning electron microscopy (SEM) with energy dispersive X-ray spectroscopy (EDX) was carried out using a Zeiss Gemini Ultra Plus microscope. The instrument was employed to examine the surface morphology and to investigate cross-sections of the anodes of the MEAs prior to and after the durability test. Specifically, the EDX probe was used to determine the bulk elemental composition distribution of the anodes. The analysis of the cross-section was performed on epoxy blocks in which the strip of the MEA was embedded.

Scanning transmission electron microscopy (STEM) with EDX was performed using an FEI (Thermo Fisher Scientific) Titan 80–200 electron microscope equipped with a probe corrector (CEOS) and an high-angle annular dark- field (HAADF) detector.[38] A probe semi-angle of 25 mrad and an inner collection angle of the detector of 70 mrad were used to achieve the "Z-contrast" conditions. For this characterization, IrO_x catalysts were removed from the MEA samples by scraping the catalyst layers with a knife edge, thereby removing as much of the catalyst layer as possible from an approximately 1cm^2 area. The specimens were

Table I. Parameters of materials of PEM water electrolyzers.

Materials	Value
Membrane type	Nafion 117®
Electrode area	17.64 cm^2
Anode catalyst (IrO_2)	$\sim$2.2 $mg_{Ir} \cdot cm^{-2}$
Cathode catalyst (Pt/C)	$\sim$0.8 $mg_{Pt} \cdot cm^{-2}$
Anode PTL	Ti felt (2GDL10–0.25, Bekaert, Belgium) a) uncoated Ti PTL for MEA_uncoated b) Ir-coated PTL for MEA_coated (0.1 $mg_{Ir} \cdot cm^{-2}$ Ir totally)
Cathode PTL	Toray paper® (TGP-H 120)

prepared by ultrasonically dispersing the catalyst in isopropyl alcohol and then depositing a drop of the suspension onto a carbon-coated Cu grid.

Atomic force microscope (AFM) measurements with a Bruker Multimode 8 (Bruker, Karlsruhe) were conducted in PF-TUNA mode, which enables simultaneous measurement of the electronic current and the nanomechanical properties. Due to the different properties of the ionomer and catalyst the technique reveals the ionomer distribution in the catalyst layer. For preparation, the MEA samples were cut with a razor blade to a size of approximately 0.5 × 0.5 cm^2 and subsequently glued to AFM steel discs with conductive carbon tape. Close to the measuring spot another conductive tape was placed to facilitate a sufficient electronic connection. Tapping was performed with 1 kHz while the current was averaged with a lock-in amplifier.

X-ray photoelectron spectroscopy (XPS) measurements were performed with a custom Scienta-Omicron HiPP-3 system operating in transmission mode and using an Al Kα X-ray (1486.6 eV) excitation source and a R4000 hemispherical analyzer. The analysis chamber pressure was maintained below 5.0 × 10^{-8} mbar, whereas the analyzer pressure was maintained at less than 1 × 10^{-9} mbar. The system was calibrated to the Au 4f region of a segment of sputter-cleaned Au foil. The X-ray source was operated with a 900 μm spot size at 300 W. Survey spectra were recorded at a pass energy of 200 eV with a slit size of 4.0 × 30 mm and a step size of 1.0 eV for an estimated energy resolution of 2.0 eV; core level measurements were performed at a 200 eV pass energy with a 0.8 × 30 mm slit size and a 0.1 eV step size, resulting in an estimated energy resolution of 0.59 eV. The C 1s, O 1s, F 1s, and S 2p core levels reported in this work are the sum of data collected at three unique areas of the sample, with measurements at each spot limited to 15 min The data was collected in this fashion in order to avoid any potential spectral artifacts due to Nafion instability under X-ray irradiation.[39,40]

Results and Discussion

Electrochemical measurements.—In this work, we investigate the effects of long-term operation on two MEAs: the MEA operated with uncoated PTL (*MEA_uncoated)*, and the MEA operated with Ir-coated PTL (*MEA_coated)*. Figure 1 shows performance results for the *cell_coated* and *cell_uncoated* sets measured at the beginning of test (BOT) and end of test (EOT), i.e., after 4000 h of operation. At BOT, the performance of *cell_coated* at 2 A·cm^{-2} was 40 mV lower than that of *cell_uncoated*. This performance change could be attributed to the use of Ir coating on the anodic PTL facing the catalyst layer. The Ir coating on the PTL reduces the ohmic resistance of the PTL/catalyst layer interface and improves cell performance. Figure 1 shows that after long term steady state operation of 4000 h, a significantly decreased performance was observed for *cell_uncoated*. The cell voltage increased by 330 mV at 0.8 A·cm^{-2}. In contrast, *cell_coated* showed identical EOT cell performance compared to BOT. The HFRs (ohmic resistances) of *cell_coated* are almost identical at the beginning and end of test (Fig. S1 in the supplementary information). However, HFR of *cell_uncoated* increased from 0.18 to 0.53 Ω cm^2 (average HFR) due to the growth of TiO_x during long-term test. In addition, the interfacial contact resistance results correspond well to the results obtained from the polarization curves (Fig. S2 in the supplementary information). The results indicate that the iridium coating mitigated the degradation processes that occurred in the cell with the uncoated PTL.

Degradation mechanism analysis.—To better understand the degradation mechanisms of an MEA on the anode side with a more sluggish process of OER, ex situ characterizations were performed on the anodes of two aged MEAs. Figure 2a shows an SEM image and EDX elemental mapping of the anode catalyst layer of the pristine MEA. The catalyst layer is dense and compact and exhibits a high degree of homogeneity. Figures 2b and 2c show the *MEA_uncoated* after 4000 h of operation demonstrated two types of areas (Fig. S3 in the supplementary information). The catalyst layer on area 1 remained attached to the membrane (Fig. 2b), whereas the other parts were detached from the membrane and remained attached to the PTL (Fig. 2c, area 2). The overview EDX mapping of the catalyst layer is shown in the supporting information (Fig. S4 in the supplementary information). The delamination of the catalyst layer was confirmed by EDX elemental mapping (Fig. 2c). The dark area of Ir mapping demonstrated the absence of the catalyst layer, whereas the brighter corresponding area in the EDX mapping of fluorine (F) and sulfur (S) displayed the exposure of the membrane. Plausible reasons for delamination of the catalyst layer were discussed in our earlier publication.[34] The delamination could originate from the tendency of polymers to adhere more strongly to oxidized surfaces than metal ones, which could be the case for the Nafion in the catalysts layer. Oxide films form much stronger bonds than metals or, if the surface is smooth due to their porosity, exhibit microscopic roughness and mechanically interlock.[41,42] TiO_x on the uncoated PTL could have a stronger adhesion to the Nafion polymer in the catalyst layer rather than smooth Ir coating on the coated PTL, which would lead to the delamination of IrO_x from the catalyst layer to the uncoated PTL surface. In contrast, Fig. 2d shows that virtually no catalyst delamination was observed in the aged *MEA_coated.* Catalyst delamination was suppressed when Ir coating was applied to the PTL. As presented in Fig. 1, *cell_coated* showed almost no decrease in cell performance, whereas *cell_uncoated* demonstrated lower cell performance. In *MEA_uncoated*, the severe delamination of the catalyst layer caused the catalyst layer material to separate or disrupt the transport pathways, which was the likely reason for the decrease in the electrochemical surface area and cell degradation.

It is worth noting that the catalyst layer delamination on the *MEA_uncoated* can be observed on the region that contacted land (highlighted in green in Fig. S5 in the supplementary information) but not on the channel regions (highlighted in yellow in Fig. S5) of the bipolar plate. The area of the delamination is estimated to be 53% − 57%. The catalyst delamination could be due to a higher contact pressure at the land vs channel region. Degradation may occur throughout the entire area of the catalyst layer. However, it may only translate into delamination where a certain pressure applies, which is the reason why the migration of catalyst layer material is a direct imprint of the cell's flow-field pattern. Mechanically induced stress and strain at PTL contact points resulted in morphological changes in the catalyst layer. It has been reported that the interfacial contact area between the catalyst layer

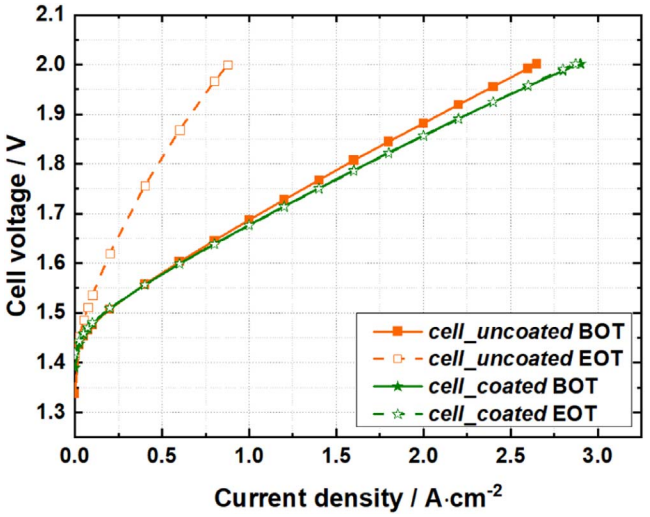

Figure 1. Polarization curves of PEM water electrolyzer single cells assembled with uncoated and coated PTLs at the beginning and end of the 4000 h durability test.

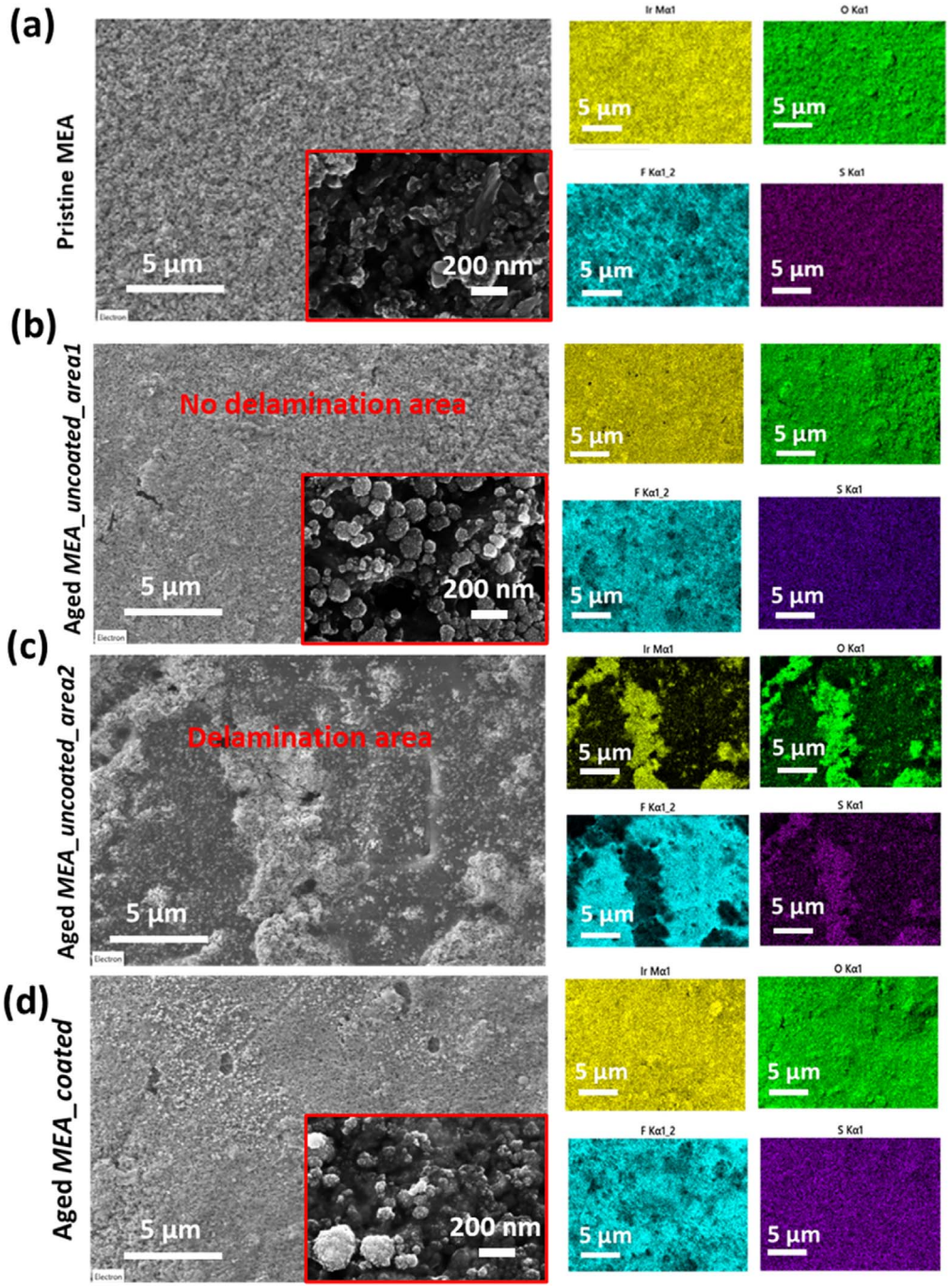

Figure 2. SEM images and EDX elemental mapping of Ir, O, F, S of (a) Pristine MEA; (b) Aged *MEA_uncoated* with no delamination area; (c) Aged *MEA_uncoated* delamination area; and (d) Aged *MEA_coated set*. Inset of (a, b, d): 200 kX magnification of SEM images.

and PTL governs the contact resistance and plays a crucial role in limiting the catalyst's utilization. Catalyst utilization is reduced due to high electric resistance in the part of the catalyst layer not in direct contact with the fibers, which lacks compression force and develops cracks.[24] Catalyst utilization could be promoted by introducing an MPL[32,33] or nanolayer[43] on the surface of the PTLs.

The inset in Fig. 2 displays the SEM images of a pristine and two aged MEAs at 200 kX magnification. Compared to pristine MEA (inset in Fig. 2a), the IrO_x particle size of both the aged MEAs increased and exhibited a more spherical and microporous structure after the long-term test (inset in Figs. 2b, 2d). Inset of Figs. 2b, 2d show that the IrO_x agglomerates of the aged MEAs were mainly spherical with diameters of 100–150 nm. Interestingly, both aged MEAs had very similar morphologies (Fig. S6 in supplementary information), indicating that whether the PTL is coated with iridium had no effect on the morphological change in the IrO_x catalysts.

Figures 3a–3c shows a cross-sectional view of the pristine MEA with a very dense and flat catalyst layer. After 4000 h of operation, parts of the catalyst layer of *MEA_uncoated* detached from the membrane and remained attached to the PTL, whereas other parts remained attached to the membrane but exhibited a curve deformation (Fig. 3d). The parts remained connected to the membrane (marked in yellow) curved at the surface and detached from the membrane, and the formation of voids and cracks was also observed (Figs. 3e and 3f). Figure 3g shows that the entire catalyst layer of *MEA_coated* remained on the membrane, but it did not connect well to it. It shows very similar curve deformation of the catalyst layer as the remaining part of the aged *MEA_coated.* The formation of voids

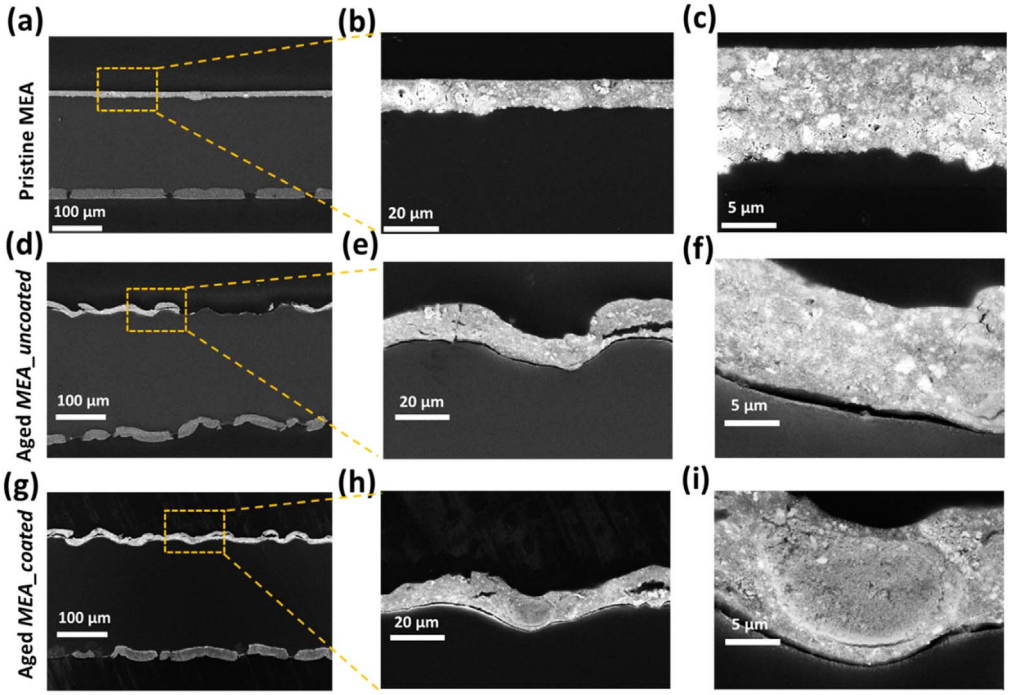

Figure 3. Cross-sectional view of the MEA images (a)–(c) Pritisne MEA; (d)–(f) Aged *MEA_uncoated*; (g)–(i) Aged *MEA_coated*.

and cracks can also be seen in Figs. 3h and 3I, which is due to Ir dissolution. [44] Ir in the catalyst layer undergoes a dissolution process but redeposited and oxidized quickly. During this process, voids in the catalyst layer can be formed.

Table II shows the thickness of the catalyst layer and the Nafion membrane before and after 4000 h of operation. The thickness of both the anode and cathode remained similar at the beginning and end of the long-term test. The thickness of the catalyst layers on both sides of the PEM seems to be unaffected by the operation, indicating the estimated metal loadings (e.g., $>2.0\ mg_{Ir}\cdot cm^{-2}$) are high enough to prevent any extensive degradation. In contrast to what has been reported for PEM fuel cells and electrolyzers,[11,45–47] no membrane thinning was observed in this study. The thickness of the Nafion membrane of a pristine MEA is 180.7 ± 1.2 μm, while it increased to 198.8 ± 20.7 μm for *MEA_uncoated* and 198.3 ± 3.5 μm for *MEA_coated* after the long-term test, respectively. Similar results were also found in our previous research[48] and another study from Siracusano et al.[8] One possible explanation for this is that the post-mortem MEAs still had residual moisture and the swelling of the membrane could not be reduced. In addition, the stressor type (hold, triangular-wave, square-wave) also plays a crucial role in degradation. In contrast to the study that performed the accelerated stress test (AST) at triangular- or square-wave cycles and found thinning of the membrane at the end of test,[14] our long-term test was performed at a constant voltage of 2 V. In PEM fuel cells, the chemical degradation of the membrane strongly depends on the operating conditions, especially the H_2 crossover, which promotes the attack of radicals. The H_2 crossover (H_2 in O_2 ratio) is lower and membrane thinning is less at higher current density.[49,50] A chemical membrane AST was run at an open circuit voltage (OCV) with a high temperature (90 °C) and low relative humidity (RH), which promoted radical attack. For the PEM electrolyzer, it is not yet fully understood which operating conditions cause and accelerate membrane thinning.[48]

Figure 4 shows the STEM and EDX elemental mapping measurements of pristine and aged MEAs. The IrO_x of the pristine MEA is around 15–20 nm. They are agglomerated and erratically distributed (Figs. 4a–4d). After 4000 h of long-term operation, the IrO_x nanoparticles of both aged MEAs showed very similar results. Compared to a pristine sample, the IrO_x of these two aged MEAs appeared to be more agglomerated and coarsened with a diameter of 100 ± 20 nm (Figs. 4e–4l). The size of IrO_x particles is quite small, around 2 nm. The Ir:O atomic ratio of the pristine MEA is 20:80, whereas the oxidation state shows a very slight change in the ratio of 26:74 and 27:73 for aged *MEA_uncoated* and *MEA coated*, respectively. The STEM and EDX elemental mapping indicate that IrO_x nanoparticles of both aged MEAs retained a relatively stable chemical state but showed a morphology change (i.e., catalyst agglomerations, spherical structures) after long-term operation. And Ir coating of the PTL doesn't have an effect in the IrO_x nanoparticles morphology and oxidation state of iridium.

The morphology change of IrO_x in the MEA after a long-term test was detected in our study, but the mechanism behind it has not yet been confirmed in the literature. A reaction-specific particle growth mechanism has not yet been identified for water electrolysis. Nanoparticles are intrinsically unstable due to their size, and particle growth always reduces the total interfacial energy. Plausible explanations for the morphology change of IrO_x include dissolution, agglomeration, and particle growth due to coalescence/redeposition.[51–53] Ir in the catalyst layer undergoes a dissolution process but redeposited and oxidized quickly. This process seems to be gradual, starting from the surface of the nanoparticles and then reaching the core. In PEM fuel cells, there are three main types of particle growth mechanisms that can also be

Table II. Average thickness of the catalyst layer and membrane before and after tests.

Average Thickness/μm	Pristine	Aged *MEA_uncoated* (not delaminated)	Aged *MEA_coated*
Anode	11.0 ± 0.8	10.5 ± 0.2	11.0 ± 2.9
Cathode	20.7 ± 1.9	19.8 ± 0.3	19.8 ± 1.6
Membrane	180.7 ± 1.2	198.8 ± 20.7	198.3 ± 3.5

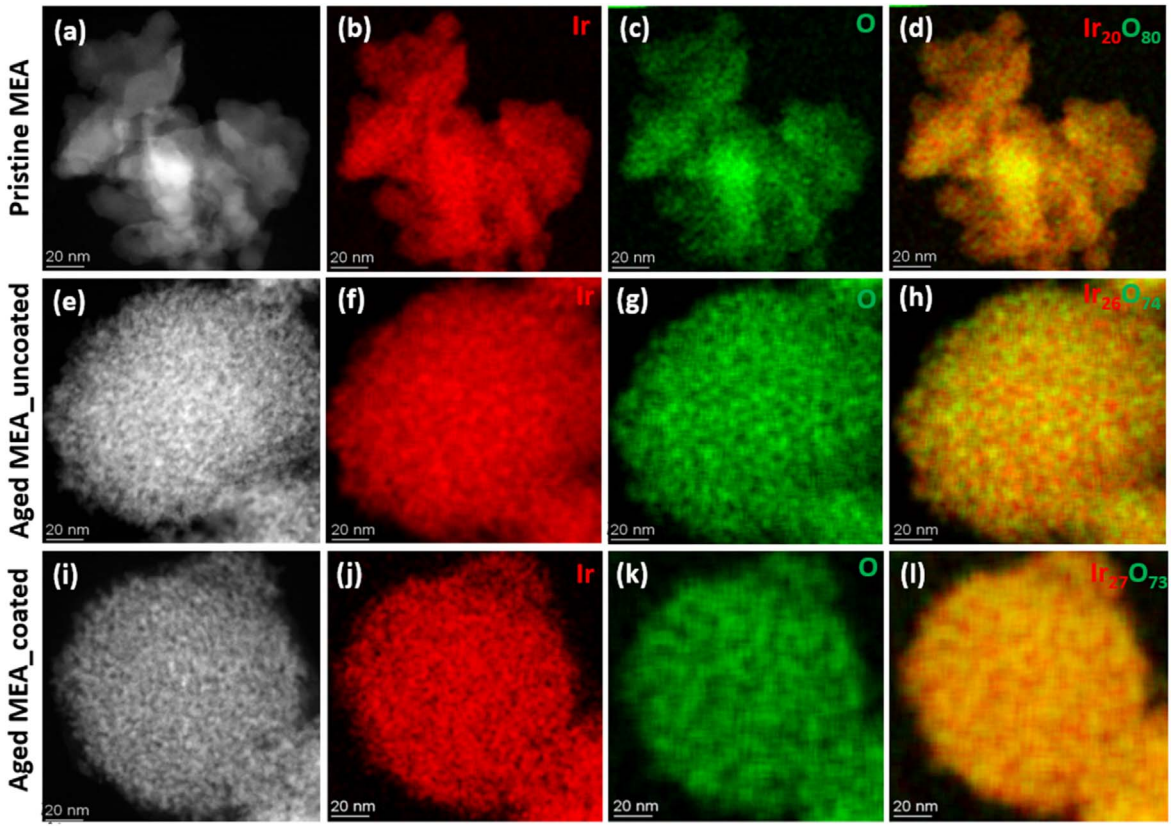

Figure 4. HAADF-STEM images of the anodic catalyst layer of the (a) Pristine MEA; (e) Aged *MEA_uncoated*; (i) Aged *MEA_coated*; (b), f), j) distribution of iridium (red) in EDX composition maps; (c, g, k) distribution of oxygen (green) in EDX composition maps; and (d), h), l) distribution of iridium and oxygen in EDX composition maps.

applied to PEM water electrolysis, namely: Ostwald ripening, re-precipitation, and coalescence, all of which can occur simultaneously or individually.[12] The Ostwald ripening and the re-precipitation mechanisms could be applied to electrolysis. In Ostwald ripening, dissolved ions are redeposited on existing particles, thus increasing the average size of them, which is reflected in the particle size distribution (PSD). During reprecipitation or redeposition, nanoparticles form at other nucleation sites (e.g., in the ionomer). Therefore, the PSD broadens, indicating variance in the sizes of the small particles formed.[12] Contrary to what we found in our study, i.e., IrO_x appeared to be more coarsened and is perhaps more amorphous in nature. Several studies from both RDE and single-cell tests reported different results regarding the change in IrO_2 morphology after durability tests, i.e., no change in the morphology of the scraped anode catalyst layer.[6,20] This suggests that different test conditions, such as the type of AST, i.e., galvanostatic or potentiostatic, constant or dynamic, and the synthesis methods of IrO_2, may have different effects on the morphology change of catalysts, leading to varied results.

In order to achieve the relative conductive area and roughness (R_a) of the MEAs, AFM measurements of the catalyst layers were performed on an area of 25 μm^2 for pristine and aged samples after the 4000 h of operation. In addition to the electronic conductivity measurements, the height and deformation were recorded simultaneously. Figure 6 displays the height, current, and deformation measurements of the pristine and aged MEAs. From the height measurements, it is apparent that the roughness changed following the long-term operation (Figs. 6a, 6d, 6g). The roughness of the pristine anode was measured as 21.2 nm, and it increased to 32.8 nm for aged *MEA_uncoated* and 39.6 nm for *MEA_coated*, respectively. A higher roughness after operation may have several origins, either the mechanical influence due to contact with the PTL or degradation or flow of the ionomer.

To gain insights into the change in the ionomer after long-term operation, the electronic conductive area and deformation of the anode surface were investigated. It was reported that the surface conductivity of the catalyst layer changed due to ionomer loss.[48] The bias was kept low enough (1 V) for mainly the electronic conductivity to be shown. Measuring ionic conductivity with AFM requires a high humidity or liquid water and a higher bias than used for this work. An increased electronic conductive area would therefore be an indication of ionomer rearrangement or degradation. For example, a decrease in ionomer layer thickness could result in a higher electronic conductive area, as thinner ionomer layers may be penetrated with the AFM tip, and a more obvious reduction in ionomer coverage. Furthermore, a higher deformation of the ionomer in comparison to the catalyst particles provides a good contrast in the AFM measurements. A lower highly deformable area would be an indication of ionomer loss or rearrangement after operation.

Figures 5b, 5e, 5h shows the electrical conductivity AFM images of the anode of pristine and aged MEAs, respectively. The IrO_x nanoparticles are distributed homogenously in the conductive areas, whereas the large non-conductive areas are associated with the ionomer. The conductive area was quantified and the values are shown in Fig. 5j. The conductive area, which is dominated by electronic conductive components of the pristine sample, exhibited a conductive area of 41%. After 4000 h of operation, the electronic conductive area of the aged *MEA_uncoated* increased to approximately 83%, indicating a loss of ionomer on the surface of the catalyst layer. A rearrangement of the catalyst layer structure by means of a flow of the ionomer due to the applied potential and high local temperature could also be possible, as well as redeposition of the catalyst onto the ionomer.[44] As the conductivity is on the same order of magnitude, the particles are connected, which supports the

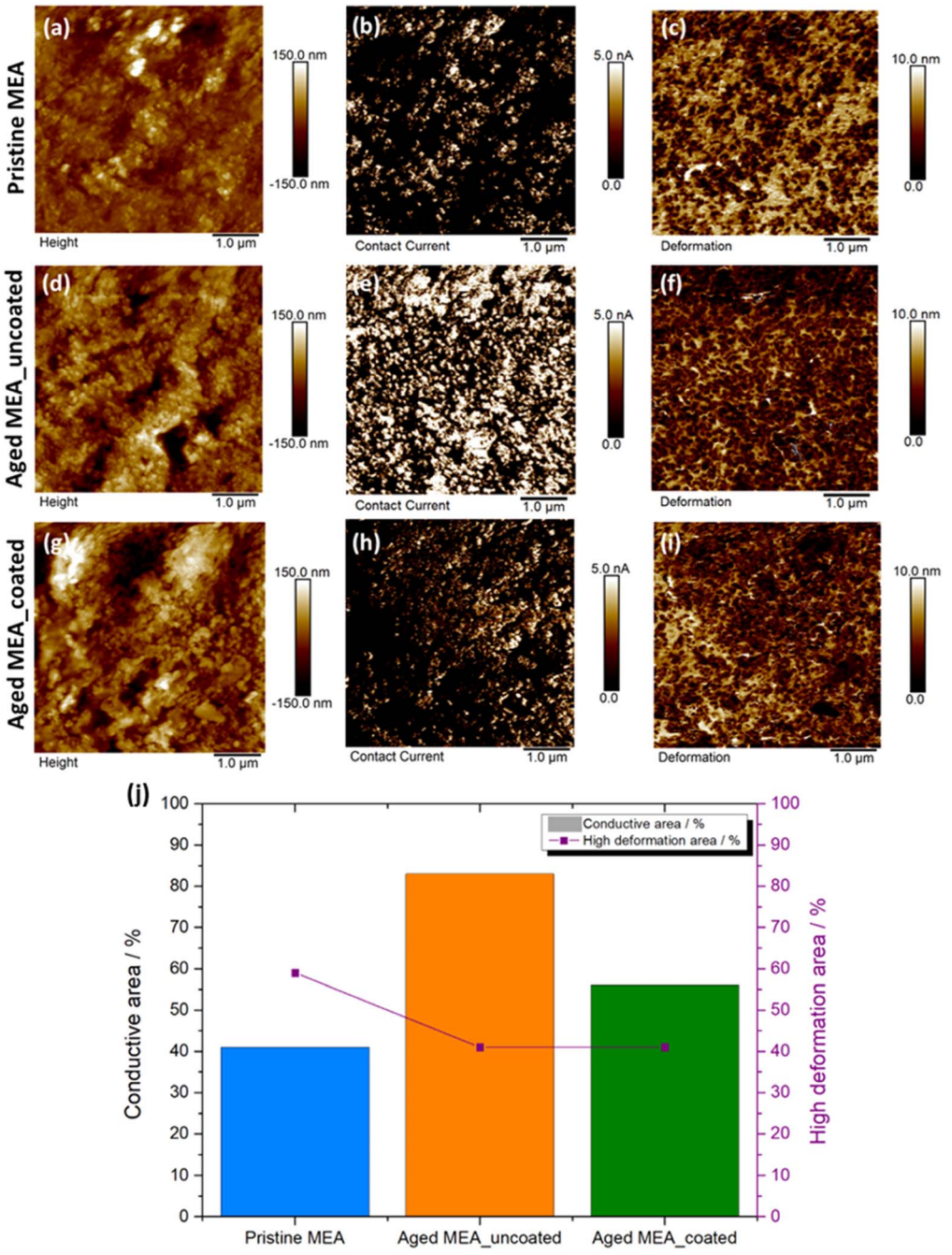

Figure 5. AFM height measurement of the: (a) Pristine MEA; (d) Aged *MEA_uncoated*; (g) Aged *MEA_coated*. AFM conductivity measurement of the: (b) Pristine MEA; (e) Aged *MEA_uncoated*; (h) Aged *MEA_coated*; AFM deformation measurement of (c) Pristine MEA; (f) Aged *MEA_uncoated*; (i) Aged *MEA_coated*; and (j) AFM conductive and deformation of the pristine and aged MEAs.

theory of a movement or loss of ionomer instead of the catalyst, whereas both theories are conceivable. In the supplementary information (Figs. S7 and S8), a typical measurement of a delaminated area is shown, which clearly shows the low magnitude of conductivity in the remaining particles. However, the conductive area of aged *MEA_coated* increased by only approximately 15% (from 41% to 56%), which indicates a lower change in the ionomer structure due to the Ir coating on the PTL. Ionomer rearrangement can be observed in the deformation channel for both aged MEAs in a decreased area with high deformation (Figs. 5f, 5i). The amount of variation in the high deformation area was fairly similar for both aged MEAs, at 18% (Fig. 5g). The performance of the electrolyzers depends on a high proton conductivity of the ionomer. The loss and degradation of ionomer in the catalyst layer will lead to a loss in performance or even the total failure of a cell. It has been found that applied voltage accelerates the degradation of ionomer, which will eventually lead to a disintegration of the catalyst layer.[19,23] Additionally, lower ionomer of the catalyst layer led to higher protonic resistance because a percolating network of the ionomer might not form.[54] Therefore, it can be expected that the cell with *MEA_uncoated* may have higher protonic resistance and lower protonic conductivity due to more severe ionomer loss, leading to higher ohmic resistance. In summary, the AFM results demonstrated that the decrease in cell performance was affected by ionomer degradation of the MEA. Although both aged MEAs featured ionomer loss and/or rearrangement after the long-term test, the Ir

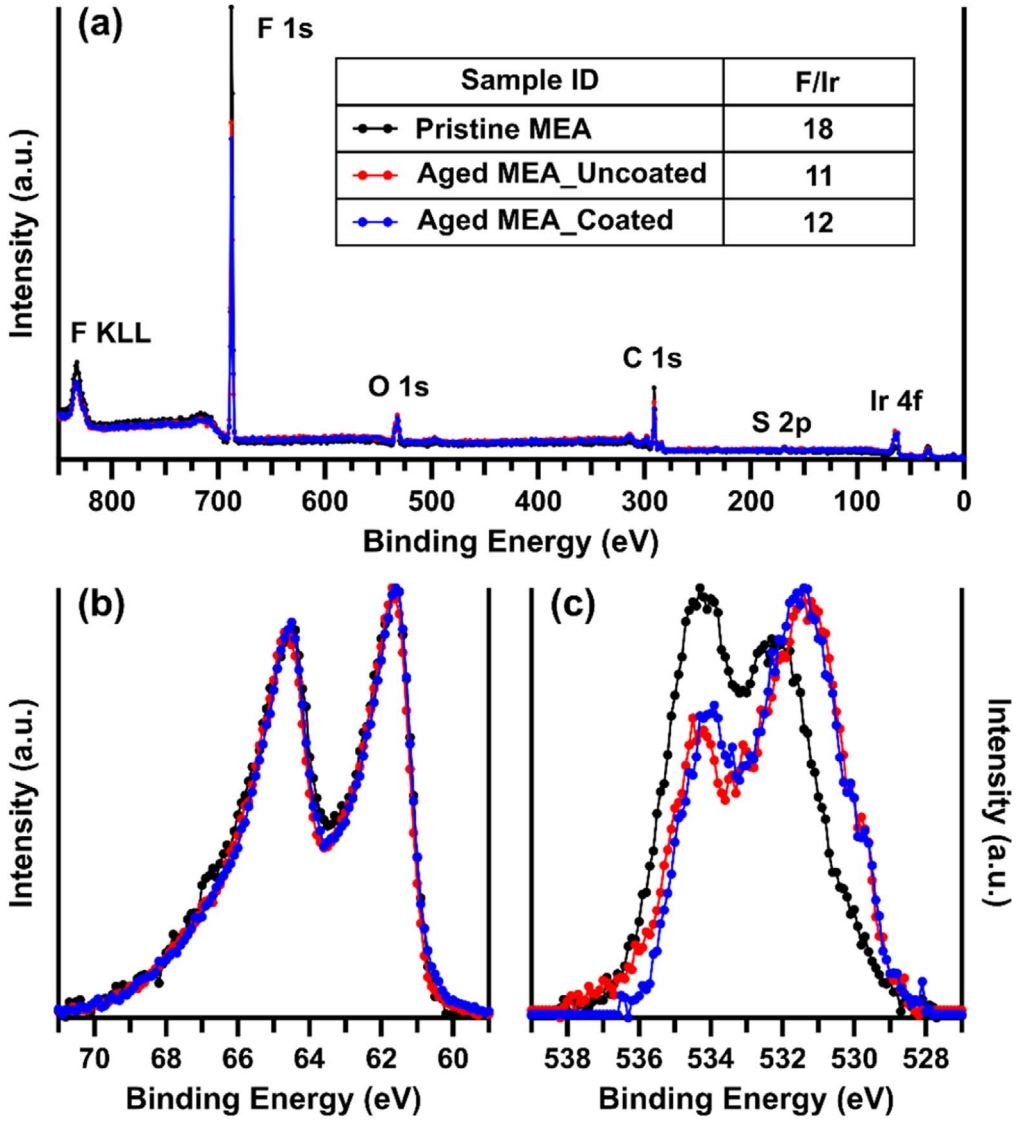

Figure 6. (a) XPS survey spectrum of pristine and aged samples are displayed alongside the F/Ir area ratios; and (b), (c) Ir 4f and O 1s core levels of pristine and aged samples are displayed with the *y*-axis scaled to normalize the minimum and maximum values.

coating at the catalyst/porous layer effectively reduced the ionomer loss of 27% of the MEA compared to the MEA assembled with an uncoated PTL when looking at the change in the electronic conductive area. From the conductive AFM measurements in Fig. 5b, 5e, and 5h, it can be seen in addition that the values of the electronic current only increased for *MEA_uncoated*.

In summary, the ionomer loss and rearrangement in the anode of the MEA can be reduced by Ir coating on the PTL from the AFM results. The reasons for less ionomer loss by adding Ir coating on the PTL can be as follows: uncoated Ti fibers with a TiO_2 passivation layer exhibit a higher electrical resistivity than Ir, which results in more Joule heating. The PTL would need to allow a greater heat flux to maintain a stable local temperature. It can be expected that the local hot spots are formed due to the poor interfacial contact and reduced thermal conductivity of the uncoated PTLs. In this case, the uncoated PTL resulted in a heterogenous temperature distribution and local hot spot formation. The ionomer loss in the catalyst layer could be accelerated if it contacts the uncoated PTL. In contrary, Ir coating added on the PTL/CL interface provides significantly higher thermal conductivity (147 W $m^{-1}\cdot K^{-1}$) than Ti (15.6–22.5 W $m^{-1}\cdot K^{-1}$) and TiO_2 (4.8–11.8 W $m^{-1}\cdot K^{-1}$).[35] During operation, the heat can be extremely easily conducted through the Ir coating, to then be further conducted away from the catalyst layer by means of both Ir coating and Ti fibers. The heat management is improved by adding Ir coating to the PTL, and so the ionomer loss for the MEA assembled with the Ir-coated PTL is less than the MEA assembled with the uncoated PTL.

XPS was performed to investigate the change of the chemical and oxidation state in the catalyst layer. Figure 6a shows the XPS survey spectra of the pristine and aged MEAs. A change in the catalyst layer composition and an enrichment in Ir was accompanied by a decrease in F signal and could be observed for both aged MEAs. The high resolution Ir 4f spectra shown in Fig. 6b displays a peak maximum of the Ir $4f_{7/2}$ at 61.6 eV, and both the position and spectral shape are in good agreement with amorphous IrO_2 reported in the literature.[55,56] Accurately deconvoluting Ir 4f to definitively identify and quantify relative amounts of different oxidation states is highly challenging due to the presence of Ir IV and Ir III satellite features that overlap the contribution of the main Ir IV and Ir III peaks. Ultimately, the pristine and aged samples showed little to no change in the Ir 4f spectral features, with only a very slight change comparing the pristine states to both aged samples present at ~63.5 eV, possibly indicating a very minor change in the Ir oxidation state, and most likely a decrease in Ir III from the pristine to aged samples. This demonstrates that despite the morphological changes being observed for IrO_x, it is very stable in terms of the

surface chemical state after long-term testing and the surface oxidation state of the catalyst is not altered, regardless of whether the MEA was assembled with coated or uncoated PTL.

Interestingly, an apparent decrease in the F:Ir ratio was observed following the long-term test. The ratio decreased from 18 to 11 for the aged *MEA_uncoated* and 18 to 12 for *MEA_coated*, indicating either a rearrangement of ionomer or dissolution of Ir. It is highly possible that these two processes occur simultaneously and affect each other. The rearrangement of ionomer was indeed observed in the AFM results in Fig. 6. Obvious changes in the O 1s were present between the pristine and aged MEAs (Fig. 6c). The clearest change is a relative decrease in 534.5 eV species (CF_2–O–CF_2) attributable to ether linkages in the Nafion side chain, indicating a decrease in ionomer surface enrichment. While the *MEA_coated* and *MEA_uncoated* samples were extremely similar, there was very slightly more of an ether signal in the *MEA_coated* sample, which is in agreement with the F/Ir ratios. Both observations suggest that the Ir coating results in a slightly lower rearrangement of Nafion ionomer. Additionally, the O 1s displays a significant change at lower binding energy of between 532 and 529 eV. After testing, significantly more signal is present from 531–529 eV. Although the sulfonic acid species terminating the Nafion side chain contributes to a signal of around 532 eV, the signal below 531 eV must be due to O coordinated with Ir, attributable to IrO_x and possible hydroxide species. As the changes observed in XPS are relative in nature, it is challenging to definitively identify whether the decrease in Nafion or increase in Ir observed is due to a change in one or both species. Several studies reported Ir dissolution and redeposition during long-term operation, resulting in the formation of the Ir band at the anode, and a diffusion of dissolved Ir into the membrane and deposition at the cathode.[13,48] However, compared to those results, no Ir was found in the cross-section of the membrane and the cathode in our study (Figs. 3d, 3g), indicating the decrease in the F:Ir ratio to be more likely due to the rearrangement of ionomer. In summary, the XPS results showed that Ir coating on the PTL reduced the loss and rearrangement of the Nafion ionomer of the MEA during the long-term operation, with no change in the Ir oxidation state.

Conclusions

The effects of the interface between the anodic catalyst and porous transport layer on the degradation of the MEA in PEM electrolyzers were investigated in this work. We found that a drastic deactivation of the MEA was apparent when the uncoated PTL was utilized, and that the uncoated PTL triggered extreme damage over the anodic catalyst layer during long-term operation. The results showed that a PGM coating between the PTL/CL interface significantly minimized the delamination and ionomer loss of the catalyst layer due to a better heat management. The uncoated PTL resulted in a heterogenous temperature distribution and local hot spot formation, which caused more ionomer loss and degradation of the catalyst layer. Despite the morphological changes like agglomeration, particle growth due to coalescence/redeposition, and the formation of voids and cracks could be identified in both aged MEAs; IrO_x is generally highly stable in terms of its chemical state, as no major changes in the Ir oxidation state was found. Additionally, Ir coating between the PTL/CL interface neither affects the morphology and the oxidation change of IrO_x in the catalyst layer during aging of MEAs. Moreover, although the ionomer loss and rearrangement of the catalyst layer were observed in both aged MEAs, our results indicate that such losses can be reduced when using the Ir coating at the PTL/CL interface. This research showed that a proper design of the PTL/CL interface is crucial not only for guaranteeing the high performance of a PEM electrolyzer, but more significantly for reducing performance degradation. This work improved understanding of the degradation mechanisms, developed superior accelerated stress tests for electrochemical devices and provided insights relevant to the electrode design, driving future optimizations of this important technology.

Acknowledgments

The authors also would like to thank Andreas Everwand and Dr. Marcin Rasinski for SEM and EDX measurements. This work makes use of the E-XPS system at the Colorado School of Mines, which was supported by the National Science Foundation under Grant No. 1626619. This work was authored in part by the National Renewable Energy Laboratory, operated by Alliance for Sustainable Energy, LLC, for the U.S. Department of Energy (DOE) under Contract No. DE-AC36–08GO28308. Funding was provided by the U.S. Department of Energy Office of Energy Efficiency and Renewable Energy (EERE) Hydrogen and Fuel Cell Technologies Office (HFTO). The views expressed in the article do not necessarily represent the views of the DOE or the U.S. Government. The U.S. Government retains and the publisher, by accepting the article for publication, acknowledges that the U.S. Government retains a nonexclusive, paid-up, irrevocable, worldwide license to publish or reproduce the published form of this work, or allow others to do so, for U.S. Government purposes. Access to the infrastructure at the Ernst Ruska-Centre, Forschungszentrum Jülich is gratefully acknowledged. Conflict of Interest. The authors declare no conflict of interest.

ORCID

Chang Liu https://orcid.org/0000-0002-4116-9246
Zhenye Kang https://orcid.org/0000-0002-1731-0705
Sarah F. Zaccarine https://orcid.org/0000-0002-7978-915X

References

1. C. Niether, S. Faure, A. Bordet, J. Deseure, M. Chatenet, J. Carrey, B. Chaudret, and A. Rouet, "Improved water electrolysis using magnetic heating of FeC–Ni core–shell nanoparticles." *Nat. Energy*, **3**, 476 (2018).
2. A. Landman, H. Dotan, G. E. Shter, M. Wullenkord, A. Houaijia, A. Maljusch, G. S. Grader, and A. Rothschild, "Photoelectrochemical water splitting in separate oxygen and hydrogen cells." *Nat. Mater.*, **16**, 646 (2017).
3. L. Yu et al., "Non-noble metal-nitride based electrocatalysts for high-performance alkaline seawater electrolysis." *Nat. Commun.*, **10**, 5106 (2019).
4. M. Carmo, D. L. Fritz, J. Merge, and D. Stolten, "A comprehensive review on PEM water electrolysis." *Int J Hydrogen Energ*, **38**, 4901 (2013).
5. L. Xia, W. Jiang, H. Hartmann, J. Mayer, W. Lehnert, and M. Shviro, "Multistep sulfur leaching for the development of a highly efficient and stable NiS_x/$Ni(OH)_2$/NiOOH electrocatalyst for anion exchange membrane water electrolysis." *Acs Appl Mater Inter*, **14**, 19397 (2022).
6. C. Rakousky, U. Reimer, K. Wippermann, M. Carmo, W. Lueke, and D. Stolten, "An analysis of degradation phenomena in polymer electrolyte membrane water electrolysis." *J. Power Sources*, **326**, 120 (2016).
7. C. Rakousky, U. Reimer, K. Wippermann, S. Kuhri, M. Carmo, W. Lueke, and D. Stolten, "Polymer electrolyte membrane water electrolysis: Restraining degradation in the presence of fluctuating power." *J. Power Sources*, **342**, 38 (2017).
8. S. Siracusano, V. Baglio, N. Van Dijk, L. Merlo, and A. S. Arico, "Enhanced performance and durability of low catalyst loading PEM water electrolyser based on a short-side chain perfluorosulfonic ionomer." *Appl. Energy*, **192**, 477 (2017).
9. Q. Feng, X. Z. Yuan, G. Y. Liu, B. Wei, Z. Zhang, H. Li, and H. J. Wang, "A review of proton exchange membrane water electrolysis on degradation mechanisms and mitigation strategies." *J. Power Sources*, **366**, 33 (2017).
10. C. Rakousky, G. P. Keeley, K. Wippermann, M. Carmo, and D. Stolten, "The stability challenge on the pathway to high-current-density polymer electrolyte membrane water electrolyzers." *Electrochim. Acta*, **278**, 324 (2018).
11. S. Siracusano, N. Van Dijk, R. Backhouse, L. Merlo, V. Baglio, and A. S. Arico, "Degradation issues of PEM electrolysis MEAs." *Renew. Energy*, **123**, 52 (2018).
12. C. Spori, J. T. H. Kwan, A. Bonakdarpour, D. P. Wilkinson, and P. Strasser, "The stability challenges of oxygen evolving catalysts: towards a common fundamental understanding and mitigation of catalyst degradation." *Angew Chem Int Edit*, **56**, 5994 (2017).
13. H. Yu, L. Bonville, J. Jankovic, and R. Maric, "Microscopic insights on the degradation of a PEM water electrolyzer with ultra-low catalyst loading." *Appl. Catalysis B*, **260**, 118194 (2020).
14. S. M. Alia, S. Stariha, and R. L. Borup, "Electrolyzer durability at low catalyst loading and with dynamic operation." *J. Electrochem. Soc.*, **166**, F1164 (2019).
15. T. Reier, M. Oezaslan, and P. Strasser, "Electrocatalytic oxygen evolution reaction (OER) on Ru, Ir, and Pt catalysts: a comparative study of nanoparticles and bulk materials." *ACS Catal.*, **2**, 1765 (2012).
16. S. M. Alia, B. Rasimick, C. Ngo, K. C. Neyerlin, S. S. Kocha, S. Pylypenko, H. Xu, and B. S. Pivovar, "Activity and durability of iridium nanoparticles in the oxygen evolution reaction." *J. Electrochem. Soc.*, **163**, F3105 (2016).
17. S. M. Alia and G. C. Anderson, "Iridium oxygen evolution activity and durability baselines in rotating disk electrode half-cells." *J. Electrochem. Soc.*, **166**, F282 (2019).

18. A. Weiß, A. Siebel, M. Bernt, T.-H. Shen, V. Tileli, and H. Gasteiger, "Impact of intermittent operation on lifetime and performance of a pem water electrolyzer." *J. Electrochem. Soc.*, **166**, F487 (2019).
19. Y. Zeng, X. Guo, Z. Shao, H. Yu, W. Song, Z. Wang, H. Zhang, and B. Yi, "A cost-effective nanoporous ultrathin film electrode based on nanoporous gold/IrO2 composite for proton exchange membrane water electrolysis." *J. Power Sources*, **342**, 947 (2017).
20. M. Povia, D. F. Abbott, J. Herranz, A. Heinritz, D. Lebedev, B.-J. Kim, E. Fabbri, A. Patru, J. Kohlbrecher, and R. Schäublin, "Operando X-ray characterization of high surface area iridium oxides to decouple their activity losses for the oxygen evolution reaction." *Energ Environ Sci*, **12**, 3038 (2019).
21. P. Jovanovič, N. Hodnik, F. Ruiz-Zepeda, I. Arčon, B. Jozinović, M. Zorko, M. Bele, M. Šala, V. S. Šelih, and S. Hočevar, "Electrochemical dissolution of iridium and iridium oxide particles in acidic media: transmission electron microscopy, electrochemical flow cell coupled to inductively coupled plasma mass spectrometry, and X-ray absorption spectroscopy study." *J. Am. Chem. Soc.*, **139**, 12837 (2017).
22. S. M. Alia, "Current research in low temperature proton exchange membrane-based electrolysis and a necessary shift in focus." *Current Opinion in Chemical Engineering*, **33**, 100703 (2021).
23. T. Morawietz, M. Handl, C. Oldani, P. Gazdzicki, J. Hunger, F. Wilhelm, J. Blake, K. A. Friedrich, and R. Hiesgen, "High-resolution analysis of ionomer loss in catalytic layers after operation." *J. Electrochem. Soc.*, **165**, F3139 (2018).
24. T. Schuler, T. J. Schmidt, and F. N. Buchi, "Polymer electrolyte water electrolysis: correlating performance and porous transport layer structure: part ii. electrochemical performance analysis." *J. Electrochem. Soc.*, **166**, F555 (2019).
25. J. Lopata, Z. Kang, J. Young, G. Bender, J. Weidner, and S. Shimpalee, "Effects of the transport/catalyst layer interface and catalyst loading on mass and charge transport phenomena in polymer electrolyte membrane water electrolysis devices." *J. Electrochem. Soc.*, **167**, 064507 (2020).
26. M. Suermann, T. Gimpel, L. V. Bühre, W. Schade, B. Bensmann, and R. Hanke-Rauschenbach, "Femtosecond laser-induced surface structuring of the porous transport layers in proton exchange membrane water electrolysis." *J. Mater. Chem. A*, **8**, 4898 (2020).
27. Z. Y. Kang et al., "Thin film surface modifications of thin/tunable liquid/gas diffusion layers for high-efficiency proton exchange membrane electrolyzer cells." *Appl. Energy*, **206**, 983 (2017).
28. C. Liu, M. Carmo, G. Bender, A. Everwand, T. Lickert, J. L. Young, T. Smolinka, D. Stolten, and W. Lehnert, "Performance enhancement of PEM electrolyzers through iridium-coated titanium porous transport layers." *Electrochem. Commun.*, **97**, 96 (2018).
29. C. Liu, K. Wippermann, M. Rasinski, Y. Suo, M. Shviro, M. Carmo, and W. Lehnert, "Constructing a multifunctional interface between membrane and porous transport layer for water electrolyzers." *Acs Appl Mater Inter*, **13**, 16182 (2021).
30. T. Bystron, M. Vesely, M. Paidar, G. Papakonstantinou, K. Sundmacher, B. Bensmann, R. Hanke-Rauschenbach, and K. Bouzek, "Enhancing PEM water electrolysis efficiency by reducing the extent of Ti gas diffusion layer passivation." *J. Appl. Electrochem.*, **48**, 713 (2018).
31. T. Schuler, J. M. Ciccone, B. Krentscher, F. Marone, C. Peter, T. J. Schmidt, and F. N. Büchi, "Hierarchically structured porous transport layers for polymer electrolyte water electrolysis." *Adv. Energy Mater.*, **10**, 1903216 (2020).
32. P. Lettenmeier, S. Kolb, F. Burggraf, A. S. Gago, and K. A. Friedrich, "Towards developing a backing layer for proton exchange membrane electrolyzers." *J. Power Sources*, **311**, 153 (2016).
33. Z. Kang, G. Yang, J. Mo, S. Yu, D. A. Cullen, S. T. Retterer, T. J. Toops, M. P. Brady, G. Bender, and B. S. Pivovar, "Developing titanium micro/nano porous layers on planar thin/tunable LGDLs for high-efficiency hydrogen production." *Int J Hydrogen Energ*, **43**, 14618 (2018).
34. C. Liu, M. Shviro, A. S. Gago, S. F. Zaccarine, G. Bender, P. Gazdzicki, T. Morawietz, I. Biswas, M. Rasinski, and A. Everwand, "Exploring the Interface of skin-layered titanium fibers for electrochemical water splitting." *Adv. Energy Mater.*, **11**, 8 2002926 (2021).
35. Z. Kang, T. Schuler, Y. Chen, M. Wang, F.-Y. Zhang, and G. Bender, "Effects of interfacial contact under different operating conditions in proton exchange membrane water electrolysis." *Electrochim Acta*, **429**, 140942 (2022).
36. T. L. Doan, H. E. Lee, S. S. H. Shah, M. Kim, C. H. Kim, H. S. Cho, and T. Kim, "A review of the porous transport layer in polymer electrolyte membrane water electrolysis." *Int. J. Energy Research*, **45**, 14207 (2021).
37. A. Laube, A. Hofer, S. Ressel, A. Chica, J. Bachmann, and T. Struckmann, "PEM water electrolysis cells with catalyst coating by atomic layer deposition." *Int. J. Hydrogen Energ.*, **46**, 38972 (2021).
38. A. Kovács, R. Schierholz, and K. Tillmann, "FEI Titan G2 80-200 Crewley." *J. large-scale research facilities JLSRF*, **2**, 43 (2016).
39. D. K. Paul, J. B. Giorgi, and K. Karan, "Chemical and ionic conductivity degradation of ultra-thin ionomer film by X-ray beam exposure." *J. Electrochem. Soc.*, **160**, F464 (2013).
40. S. A. Mauger, M. Wang, F. C. Cetinbas, M. J. Dzara, J. Park, D. J. Myers, R. K. Ahluwalia, S. Pylypenko, L. Hu, and S. Litster, "Development of high-performance roll-to-roll-coated gas-diffusion-electrode-based fuel cells." *J. Power Sources*, **506**, 230039 (2021).
41. J. D. Venables, "Adhesion and durability of metal-polymer bonds." *J. Mater. Sci.*, **19**, 2431 (1984).
42. L. P. Buchwalter, "Adhesion of polyimides to metals and metal oxides." *J. Adhes. Sci. Technol.*, **1**, 341 (1987).
43. G. Yang, S. Yu, Z. Kang, Y. Li, G. Bender, B. S. Pivovar, J. B. Green Jr, D. A. Cullen, and F. Y. Zhang, "Building electron/proton nanohighways for full utilization of water splitting catalysts." *Adv. Energy Mater.*, **10**, 16 1903871 (2020).
44. S. F. Zaccarine, M. Shviro, J. N. Weker, M. J. Dzara, J. Foster, M. Carmo, and S. Pylypenko, "Multi-scale multi-technique characterization approach for analysis of pem electrolyzer catalyst layer degradation." *J. Electrochem. Soc.*, **169**, 064502 (2022).
45. S. A. Grigoriev, K. A. Dzhus, D. G. Bessarabov, and P. Millet, "Failure of PEM water electrolysis cells: Case study involving anode dissolution and membrane thinning." *Int J Hydrogen Energ*, **39**, 20440 (2014).
46. B. Wu, M. Zhao, W. Shi, W. Liu, J. Liu, D. Xing, Y. Yao, Z. Hou, P. Ming, and J. Gu, "The degradation study of Nafion/PTFE composite membrane in PEM fuel cell under accelerated stress tests." *Int J Hydrogen Energ*, **39**, 14381 (2014).
47. S. Zhang, X.-Z. Yuan, J. N. C. Hin, H. Wang, K. A. Friedrich, and M. Schulze, "A review of platinum-based catalyst layer degradation in proton exchange membrane fuel cells." *J. Power Sources*, **194**, 588 (2009).
48. P. Lettenmeier et al., "Durable membrane electrode assemblies for proton exchange membrane electrolyzer systems operating at high current densities." *Electrochim. Acta*, **210**, 502 (2016).
49. M. Bernt, J. Schröter, M. Möckl, and H. Gasteiger, "Analysis of gas permeation phenomena in a PEM water electrolyzer operated at high pressure and high current density." *J. Electrochem. Soc.*, **167**, 124502 (2020).
50. J. A. Wrubel, C. Milleville, E. Klein, J. Zack, A. M. Park, and G. Bender, "Estimating the energy requirement for hydrogen production in proton exchange membrane electrolysis cells using rapid operando hydrogen crossover analysis." *Int. J. Hydrogen Energ.*, **47**, 28244 (2022).
51. G. C. da Silva, K. J. Mayrhofer, E. A. Ticianelli, and S. Cherevko, "The degradation of Pt/IrOx oxygen bifunctional catalysts." *Electrochim Acta*, **308**, 400 (2019).
52. H. Yu, N. Danilovic, Y. Wang, W. Willis, A. Poozhikunnath, L. Bonville, C. Capuano, K. Ayers, and R. Maric, "Nano-size IrOx catalyst of high activity and stability in PEM water electrolyzer with ultra-low iridium loading." *Appl. Catalysis B*, **239**, 133 (2018).
53. S. Cherevko, "Stability and dissolution of electrocatalysts: Building the bridge between model and 'real world' systems." *Curr. Opin. Electrochem.*, **8**, 118 (2018).
54. M. Mandal, M. Moore, and M. Secanell, "Interfaces, Measurement of the protonic and electronic conductivities of PEM water electrolyzer electrodes." *ACS Applied Materials*, **12**, 49549 (2020).
55. V. Pfeifer, T. E. Jones, J. J. Velasco Vélez, C. Massué, R. Arrigo, D. Teschner, F. Girgsdies, M. Scherzer, M. T. Greiner, and J. Allan, "The electronic structure of iridium and its oxides." *Surf. Interface Anal.*, **48**, 261 (2016).
56. P. Lettenmeier, J. Majchel, L. Wang, V. A. Saveleva, S. Zafeiratos, E. R. Savinova, J. J. Gallet, F. Bournel, A. S. Gago, and K. A. Friedrich, "Highly active nano-sized iridium catalysts: synthesis and operando spectroscopy in a proton exchange membrane electrolyzer." *Chem. Sci.*, **9**, 3570 (2018).